HHS Public Access

Author manuscript

Nat Chem Biol. Author manuscript; available in PMC 2018 December 04.

Published in final edited form as:

Nat Chem Biol. 2018 July ; 14(7): 655–663. doi:10.1038/s41589-018-0062-z.

Copper regulates rest-activity cycles through the locus coeruleus-norepineprhine system

Tong Xiao[1,3], **Cheri M Ackerman**[1,3], **Elizabeth C Carroll**[2,#], **Shang Jia**[1,3], **Adam Hoagland**[2], **Jefferson Chan**[1,3], **Bao Thai**[2,3], **Christine S Liu**[1,3], **Ehud Y Isacoff**[2,4], and **Christopher J Chang**[1,2,3,4,*]

[1]Department of Chemistry, University of California, Berkeley, CA 94720, USA

[2]Department of Molecular and Cell Biology, University of California, Berkeley, CA 94720, USA

[3]Howard Hughes Medical Institute, University of California, Berkeley, CA 94720, USA

[4]Helen Wills Neuroscience Institute, University of California, Berkeley, CA 94720, USA

Abstract

The unusually high demand for metals in the brain along with insufficient understanding of how their dysregulation contributes to neurological diseases motivates the study of how inorganic chemistry influences neural circuitry. We now report that the transition metal copper is essential for regulating rest–activity cycles and arousal. Copper imaging and gene expression analysis in zebrafish identifies the locus coeruleus-norepinephrine (LC-NE) system, a vertebrate-specific neuromodulatory circuit critical for regulating sleep, arousal, attention, memory and emotion, as a copper-enriched unit with high levels of copper transporters CTR1 and ATP7A and the copper enzyme dopamine beta-hydroxylase (DBH) that produces NE. Copper deficiency induced by genetic disruption of ATP7A, which loads copper into DBH, lowers NE levels and hinders LC function as manifested by disruption in rest–activity modulation. Moreover, LC dysfunction caused by copper deficiency from ATP7A disruption can be rescued by restoring synaptic levels of NE, establishing a molecular CTR1-ATP7A-DBH-NE axis for copper-dependent LC function.

*Corresponding author. chrischang@berkeley.edu (C.J.C.).

#Current address: Department of Imaging Physics, Delft University of Technology, Lorentzweg 1, 2628 CJ Delft, The Netherlands. Correspondence and requests for materials should be addressed to C.J.C.

Author Contributions

T.X. and C.J.C. designed research; T.X., C.M.A., E.C., and A.H. performed imaging and behavioral assays; T.X., C.M.A., and B.T. performed copper imaging and analysis assays; S. J. and J. C. synthesized and characterized fluorescent copper probes; T.X. and C.S.L. conducted *in situ* hybridization and IHC assays; T.X., C.M.A., E.C., and C.J.C. wrote the manuscript; E.Y.I. provided valuable input on the manuscript.

Competing Financial Interests

The authors declare no competing financial interests.

Any supplementary information and source data are available in the online version of the paper.

INTRODUCTION

For reasons that remain insufficiently understood, the unique biology of the brain as the center of consciousness is underpinned by its unique chemistry of accumulating select elements at higher concentrations than anywhere else in the body[1,2]. These include redox-active transition metals like copper and iron[2], in part because the brain is the body's most oxidatively active organ, comprising just 2% of body weight but requiring 20% of oxygen consumption. However, the brain's dependence on metals for normal function may be a double-edged sword, as the same potent redox activity of copper and iron can trigger oxidative stress and damage, leading to neurodegeneration[2–7].

Copper distributions in the brain are spatially diverse and change with age and nutritional status[8]. In the human brain, the locus coeruleus (LC) acquires *ca.* 10 times higher copper concentrations compared to other brain regions[2,9,10] and is particularly vulnerable in many neurodegenerative diseases, including Alzheimer's, Parkinson's and Huntington's diseases [11–13]. At the cellular level, copper pools are regulated by several copper transporters[14,15], including the high affinity copper transporter, CTR1 (also known as SLC31A1), as well as metallochaperones that deliver copper to various destinations within the cytosol and organelles[16–18]. In this context, the copper-dependent ATPases ATP7A and ATP7B serve the dual purpose of metalating proteins and/or controlling copper efflux from the cell[4,19]. Despite advances in the field, molecular and cellular mechanisms of how homeostatic control of brain copper influences behavior remain insufficiently understood.

To study how transition metals are utilized in the brain, we focused on the copper-rich LC region, which has broad projections throughout the central nervous system. In mammals, the LC is considered to play major roles in regulating sleep, arousal, learning, attention, mood, and fear responses[20,21]. The chemistry of the LC is dominated by catecholamines, and their imbalance contributes to severe psychiatric disorders[22]. The two types of catecholamines present in the LC, dopamine (DA) and norepinephrine (NE), share a common biosynthetic pathway, up to a final step during which the copper-dependent enzyme dopamine beta-hydroxylase (DBH)[23–25] converts DA to NE. DBH is metalated by the P-type copper-transporting ATPase, ATP7A[26]. The LC is the major source of NE to the central nervous system (CNS), and levels of NE in the mammalian brain are higher than those of DA, even though DA neurons greatly outnumber their NE counterparts[27]. Unlike DA and serotonin (5-hydroxytrypamine, 5-HT), NE is unique to vertebrates[28–30]; however, when the LC-NE system emerged during evolution remains unclear.

Against this backdrop, we utilized zebrafish as a model organism to study metal-dependent brain chemistry. Here we report an essential role for copper in the brain in regulating sleep-related and arousal behaviors through the LC-NE system. Metal imaging studies using a pair of newly developed fluorescent copper probes along with Laser Ablation Inductively Coupled Plasma Mass Spectrometry (LA-ICP-MS) reveal enrichment of copper in brain neurites/neuropils rather than cell bodies. Complementary *in situ* hybridization studies show high levels of copper transporters CTR1 and ATP7A along with the copper enzyme DBH localized to the LC. Copper deficiency induced by genetic manipulation of ATP7A shows that this metal is critical for LC-mediated rest–activity balance and arousal response and that

this effect is associated with regulation of synaptic NE, the product of copper-dependent DBH catalysis. Phylogenetic analysis shows that development of the LC-NE is assisted by evolution of more specialized copper transporters in Gnathostomata vertebrates through gene duplication of ATP7 into ATP7A and ATP7B. Taken together, the data identify an essential role for copper in the evolution and function of the LC-NE through a molecular CTR1-ATP7A-DBH-NE axis, including a role for copper in the regulation of sleep-related and arousal behaviors.

RESULTS

Imaging labile copper in the zebrafish brain

As a starting point for our investigations, we sought to visualize distributions of labile copper within the brains of these living organisms, as previous *in vivo* copper imaging studies were limited primarily to liver detection[31,32]. To meet this goal, we designed and synthesized Copper Fluor-4 (CF4; **1**) and Control Copper Fluor-4 Sulfur 2 (Ctrl-CF4-S2; **2**), a pair of unique molecular probes that, when used in concert, can enable detection of labile copper pools in small living organisms (Fig. 1a). CF4 is a Cu^{+}-specific fluorescent sensor based on a rhodol dye scaffold that displays a 10-fold turn-on response to copper that is stable in a physiologically relevant pH regime between 6 and 8 (Supplementary Fig. 1) with high copper selectivity, particularly over zinc and iron as well as abundant cellular alkali and alkaline earth metals (Fig. 1b), a 1:1 Cu^{+}:probe binding stoichiometry, and an apparent dissociation constant (K_d) of 2.9×10^{-13} M (Supplementary Fig. 2, Supplementary Table 1). The introduction of a six-membered piperidine group on the xanthenone ring of the rhodol affords a probe with good cellular retention and high signal-to-noise ratio to image copper within whole living organisms.

A key chemical advance is in the development of Ctrl-CF4-S2, which utilizes the same dye scaffold as CF4 but does not respond to copper owing to its modified isosteric receptor (Supplementary Fig. 3). Like previously reported control probes for labile copper imaging in cells, Ctrl-CF4-S2 is comparable in size, shape and hydrophobicity to its parent copper probe CF4. However, a subtle but important chemical difference that enables the expansion of this concept to *in vivo* use is that just two of the four thioether ligands in the copper-responsive CF4 receptor are replaced with methylene groups, rather than changing all four sulfur donors to carbons as reported in previous designs. The resulting Ctrl-CF4-S2 compound bears an NS_2C_2 receptor that exhibits greater *in vivo* permeability for use in living organisms (Supplementary Fig. 4). Indeed, the analogous Control Copper Fluor-4 (Ctrl-CF4, **9**) compound with an NC_4 receptor does not penetrate beyond the skin of zebrafish, while the new Ctrl-CF4-S2 control dye permeates the fish and shows comparable *in vivo* distribution to the parent CF4 indicator (Supplementary Fig. 4). As in live zebrafish, the uptake ratio of CF4 and Ctrl-CF4-S2 is comparable in HEK cells, a standard cell model for evaluating fluorescent probes (Supplementary Fig. 5)

We then applied CF4 and Ctrl-CF4-S2 to visualize labile copper pools in developing zebrafish embryos (Fig. 1c). The CF4 signal appears strongly associated with neuropils, extracellular matrix and ventricles, but is excluded from the nuclei of cells. Copper supplementation of fish with 100 μM Cu(histidine)$_2$ for 30 min results in a statistically

significant increase in CF4 fluorescence, while copper deficiency induced by overnight treatment of fish with 500 μM of the copper chelator bathocuproine disulfonate (BCS) decreases the CF4 signal (Fig. 1d). In both HEPES buffer and cell lysates, CF4 showed strong dose-dependent responses to copper (Supplementary Figs. 6 and 7). In contrast, we observed no significant changes in Ctrl-CF4-S2 fluorescent signals with either Cu(histidine)$_2$ or BCS addition (Fig. 1d), suggesting that labile pools of copper in the developing zebrafish brain are localized to neural processes and brain ventricles. Taken together, the data establish that CF4 and Ctrl-CF4-S2 can be used in concert to assess changes in labile copper distributions in small living organisms such as zebrafish, and that subtle design changes in receptors can create effective control probe and probe pairs for *in vivo* use.

A dynamic copper distribution in the developing brain

To provide a more direct measure of copper distributions in the developing zebrafish brain, we employed LA-ICP-MS[33,34] on flash-frozen tissues to map total brain copper pools with spatial resolution (Fig. 2, Supplementary Fig. 8). These studies reveal that copper distribution is spatially and temporally regulated in the developing zebrafish brain, with copper concentrations varying among brain regions and steadily rising throughout development. In line with previous studies in rodents suggesting that brain copper is concentrated in the neuropil within synaptic vesicles[35–37], we observed elevated copper levels in larvae and adults within neuropils and fascicles, rather than somata, of neurons (Supplementary Fig. 9). Moreover, these data are consistent with CF4 and Ctrl-CF4-S2 molecular imaging of labile copper pools. As a representative example illustrating the dynamic nature of brain copper distributions during development, we focused on the tectal neuropil, which is the largest neuropil containing a high density of neurites. We analyzed the copper signals at developmental stages before and after neurite innervation and found that copper levels in the tectum are low (<0.5 ppm) at 2 days post fertilization (dpf), a developmental time-point at which no neurites have reached this region (Supplementary Fig. 8), and that the copper concentrations rise in concert with progressive neurite innervation at 4 dpf (Supplementary Fig. 8) and 6 dpf (Fig. 2a–d), reaching 1.5 ppm Cu. In contrast, analogous LA-ICP-MS imaging of zinc shows the opposite cellular distribution to copper, with highest observed zinc levels concentrated within cell bodies, but little detectable signal in neuropils or fascicles (Supplementary Fig. 10).

The ATP7A mutant has reduced copper levels in the brain

To study how copper regulates brain function, we employed a genetic model of copper dysregulation, *Calamity*$^{gw71-/-}$ (*Cal*^{gw71}). *Cal*^{gw71} mutants bearing a hypomorphic allele of the *atp7a* gene[38] are morphologically indistinguishable from their wildtype siblings under normal rearing conditions – embryo medium or system water reconstituted from instant ocean salt, which contains approximately 1.8 μmol/kg of copper (**Online Methods**). Interestingly, LA-ICP-MS copper mapping establishes that not only are overall brain copper levels lower in *Cal*^{gw71} fish compared to their wildtype counterparts (Fig. 2e–g, Supplementary Fig. 8), but dramatic decreases are observed in neuropil and fascicle regions ($P<0.001$ at 4 dpf and 6 dpf quantified in the tectal neuropil, N=18 for each group). This copper deficiency is spatially selective, as total larval copper concentrations in *Cal*^{gw71} (0.87

μg Cu/g tissue) vs wildtype (0.92 μg Cu/g tissue) fish at 5–6 dpf are comparable, suggesting that reduction of ATP7A function causes selective disruption in copper accumulation in the brain. In contrast, zinc levels in *Cal*^{gw71} mutants remain unchanged from wildtype (Supplementary Fig. 11).

Copper modulates rest–activity cycles

Next, we investigated changes in the labile copper pool in *Cal*^{gw71} mutants with CF4 (Fig. 3a, Supplementary Fig. 12). Similar to larvae treated with the copper chelator BCS, we observed decreases in CF4 fluorescence signals in the brains of *Cal*^{gw71} mutants compared to wildtype controls. Having characterized brain copper pools in developing zebrafish through a combination of labile copper and total copper imaging using molecular probes and LA-ICP-MS, respectively, we next evaluated functional roles for this metal in neural circuitry. In particular, we explored the potential contributions of copper to arousal behaviors in simple model organisms, inspired by the fact that rest-wake disorders observed in some patients with genetic disorders of copper metabolism remain insufficiently understood[39].

As our imaging experiments establish that the brains of *Cal*^{gw71} mutants are copper deficient, we analyzed rest-activity behaviors in this model. High speed recording of spontaneous swimming during the day show that *Cal*^{gw71} mutants, which are viable[38] and fertile, have comparable locomotion in terms of swimming speed and frequency to the wildtype controls (Supplementary Fig. 13). Characterization of the circadian activities of wildtype larvae and *Cal*^{gw71} mutants (pooled from siblings and cousins), however, revealed distinct differences. Between 4.5 and 6.5 dpf, under a controlled light–dark cycle that mimicked a 14 hr day and 10 hr night, wildtype larvae cycled in swim activity between higher frequency of swim bouts during the day and lower frequency at night (Supplementary Fig. 14). In contrast, we observed that *Cal*^{gw71} mutants are more active at night and less active during the day compared to wildtype controls (Fig. 3b, Supplementary Fig. 14).

To further investigate whether dysregulation in brain copper homeostasis triggers additional sleep-related behavioral changes, we studied the acoustic startle responses (ASR)[40] at a range of sound intensities during different phases of the circadian cycle. Similar to previous studies[41], we observed that wildtype larvae have lower maximal escape responses during day than night (Fig. 3c). This difference is not due to lighting conditions but instead is dependent upon circadian cycles (Supplementary Fig. 15). In contrast, maximal escape responses of *Cal*^{gw71} mutants are indistinguishable between day and night (Fig. 3d). The behavioral differences between wildtype and *Cal*^{gw71} mutants are consistent for siblings and cousins (Supplementary Fig. 16, Fig. 3c,d). Together, these results suggest that *Cal*^{gw71} mutants have altered spontaneous swim activities and arousal behaviors during circadian cycles.

To verify that the circadian behavioral changes observed in *Cal*^{gw71} mutants are a direct cause of brain copper deficiency, we reduced brain copper levels through pharmacological interventions. We previously showed through imaging that BCS incubation significantly reduces labile brain copper, and as such, we performed the circadian ASR assay with BCS-treated wildtype larvae and controls (Supplementary Fig. 17). Larvae were treated with 500 μM BCS from 3–6 dpf. LA-ICP-MS measurements confirmed that BCS-treated fish have

reduced total brain copper compared to wildtype (Fig. 3e), but zinc levels remain unchanged (Supplementary Fig. 18). Whereas vehicle-treated controls display lower maximal escape responses during day than night (Fig. 3f), BCS-treated larvae exhibit indistinguishable ASR curves during the day and night (Fig. 3g). These data indicate that BCS-treatment of wildtype fish recapitulates behavioral deficits in *Cal*^{gw71} mutants, suggesting that maintaining copper homeostasis is essential for modulating behaviors related to circadian cycles and sleep.

Copper transporters are enriched in LC neurons

With data showing that copper is essential for regulating rest–activity and arousal responses, we sought to identify the neural circuitry and molecular targets of how this metal contributes to these fundamental behaviors by directly analyzing expression patterns of genes involved in copper trafficking. We performed *in situ* hybridization for three major copper transporter genes, *ctr1*, *atp7a*, and *atp7b* in zebrafish larvae. The results show that both *ctr1* and *atp7a* expression patterns are indeed highly spatially regulated (Fig. 4a,b) and that their expression patterns highly resemble that of *dbh* (Fig. 4c), which marks the LC neurons. This pattern of expression is established by 3 dpf and maintained through adulthood (Supplementary Fig. 19). Similarly, *in situ* hybridization data from the Allen Mouse Brain Atlas also shows that *ctr1* is highly expressed in the mouse LC, but is barely detectable in other brain regions[42]. To confirm the identity of the *ctr1*- and *atp7a*-expressing neurons, we analyzed two transgenic reporter lines, *Tg(dbh:GFP)* and *Tg(dbh:mCherry)* where GFP or mCherry expression is driven by the *dbh* promoter[43]. By using fluorescent *in situ* hybridization for *dbh*, *ctr1*, and *atp7a* mRNA and immunofluorescence staining for GFP/mCherry, we verified that GFP/mCherry expression patterns faithfully reflect the endogenous expression pattern of *dbh* (Fig. 4d–f), and co-localize with *ctr1* (Fig. 4g–i) and *atp7a* (Fig. 4j–l). The results establish that molecular targets for copper import (CTR1), copper-dependent NE synthesis (DBH), and copper export and metalloprotein metalation (ATP7A) are highly and specifically enriched in the LC.

Copper modulates rest–activity cycles through the LC

One of the major roles for the LC in the mammalian brain is to regulate sleep-wake cycles[20,44]. LC is also the brain region with the highest concentration of copper[2,9]. With data showing that LC is the circuitry that contains the highest expression of copper-trafficking genes in the brain, we asked whether LC is necessary for rest–activity cycles regulated by copper homeostasis by using 2-photon laser ablation with *Tg(dbh:mCherry)* fish to selectively remove LC cells while leaving the rest of the brain intact.

To determine the time course for ablation and behavior analysis, we characterized the development of LC during the embryonic/larval stage (Supplementary Fig. 20). At 2 dpf, 0–9 LC cell bodies are found per hemi-brain in rhombomere 1. We observed heterogeneity in sibling animals (Supplementary Fig. 21), with little correlation in number of cells between the left and right side (Supplementary Fig. 22) within the same fish, suggesting that epigenetic factors beyond genetic control might contribute to LC cell number. By tracking the cells from 2–7 dpf, we observed little change in cell count (Supplementary Fig. 23), which indicates cell differentiation is complete and no new LC cells are added to the

circuitry. Based on this information, we performed the LC ablation at 3.5–4 dpf and behavioral analysis at 5–7 dpf (Supplementary Fig. 24). Efficacy of the laser ablation was confirmed by imaging after the behavioral analysis (Supplementary Fig. 25).

First, we performed circadian ASR analysis. In contrast to wildtype sham controls, which display lower maximal responses during the day than night (Fig. 5a), LC-ablated larvae show elevated ASR maximal responses during the day, which are comparable to maximal responses during the night. When tested for circadian activities (Fig. 5b), between 4.5 and 6.5 dpf, wildtype larvae with intact LC displayed higher swim activity during the day and lower activity at night, under a controlled light–dark cycle (Fig. 5c). In contrast, LC-ablated larvae were more active at night and less active during the day than their LC-intact siblings (Fig. 5c,d and Supplementary Fig. 26), similar to the changes observed in the copper-deficient *Cal*^{gw71} mutants. The largest differences between the groups were the changes in activity at the dawn transitions (Fig. 5d). These data establish that the LC region is necessary for maintaining normal rest–activity cycles in larval zebrafish.

To ask whether rest–activity changes in *Cal*^{gw71} mutants are caused by diminished LC function, we also ablated LC cells in *Cal*^{gw71} mutants. In circadian ASR analysis, LC-ablated *Cal*^{gw71} mutants and sham control *Cal*^{gw71} mutants exhibit similar response curves (Fig. 5e,f). Similarly, circadian activities are also comparable between LC-ablated and sham control *Cal*^{gw71} mutants (Supplementary Fig. 27). The results suggest that rest–activity deficits in *Cal*^{gw71} mutants are caused by compromised LC function.

Copper modulates rest–activity cycles via norepinephrine

To investigate the molecular mechanisms of how copper regulates sleep-related behavior, we used a candidate target approach. Because the LC expresses high levels of the copper-containing enzyme DBH, which is the terminal enzyme in the biosynthesis of NE from DA, we hypothesized that these rest–activity phenotypes could operate through a mechanism where reduced DBH activity results in lower NE levels (Fig. 6a). To determine whether DBH activity may cycle with circadian rhythm, we performed RT-PCR on wildtype larvae and found that mRNA expression of *dbh* peaks before dawn (Supplementary Fig. 28), whereas the mRNA expression of *atp7a* is constant (Supplementary Fig. 29). The DBH enzyme requires a copper cofactor to catalyze the production of NE; thus, we asked whether a change in copper homeostasis would affect NE production. As expected, we observed a 37% decrease in NE:DA ratio (wildtype larvae: 17.4 ng/ml NE; 2.46 ng/ml DA; *Cal*^{gw71} mutants: 12.9 ng/ml NE; 2.91 ng/ml DA) in copper-deficient *Cal*^{gw71} homozygotes compared to wildtype larvae at 6 dpf (Fig. 6b), consistent with the role of ATP7A in delivering copper to activate DBH for NE synthesis. The expression of DBH is comparable between *Cal*^{gw71} homozygotes compared to wildtype larvae (Supplementary Fig. 30). This result led to the prediction that LC function would be compromised in the copper-deficient mutant due to lower levels of NE at synapses compared to wildtype congeners through loss of DBH activity.

As a further test of this model, we asked whether atomoxetine, an inhibitor of norepinephrine transporter (NET, also known as Slc6a2)-mediated NE reuptake that prolongs residence of NE in the synapse[45], could rescue the circadian cycle behavioral

deficit in the copper-deficient *Cal*^{gw71} mutant. Indeed, in circadian ASR analysis, atomoxetine-treated *Cal*^{gw71} mutants showed decreased maximal responses during the day (Fig. 6c) and night (Fig. 6d). In contrast, atomoxetine did not change ASR curves in wildtype (Fig. 6e,f). Furthermore, we also observed a partial restoration of the rest-activity transition in *Cal*^{gw71} larvae that were exposed from 4.5 dpf to atomoxetine (Fig. 6g,h), as well as a modest decrease in nighttime activity. These results provide evidence that both rest and activity states are regulated by NE, likely from a copper-dependent molecular ATP7A-DBH axis. Taken together with the metal imaging and behavioral observations on copper-deficient and LC-deficient fish, the data support a model in which copper enters LC neurons through CTR1 and is loaded into DBH through ATP7A for subsequent NE synthesis and synaptic action, defining a CTR1-ATP7A-DBH-NE molecular pathway for copper-based modulation of sleep-related behavior.

Parallel evolution of norepinephrine and copper pathways

Finally, to identify the key time-point in evolution when NE became a major brain neuromodulator in the CNS, we performed phylogenetic analysis of genes unique for NE biosynthesis and reuptake relative to the other major monoamine neurotransmitters dopamine (DA) and serotonin (5-HT) in parallel to genes involved in copper homeostasis. Specifically, we focused on ATP7A, which loads copper into DBH[23–25] (Fig. 6a, Supplementary Fig. 31). Along these lines, all invertebrates have a single *atp7* gene, whereas vertebrates have two paralogous *atp7* genes, *atp7a* and *atp7b*, which appeared in Agnathans due to a gene duplication event in early chordates (Supplementary Fig. 32). Interestingly, this gene duplication in copper transport is accompanied by appearance of the NE transporter, NET/Slc6a2, in Gnathostomata (Supplementary Fig. 31). NET resides at the presynaptic terminal for re-uptake of NE from the synaptic cleft. We suggest that these newly acquired genes in both copper homeostasis and NE synthesis/transport in early vertebrates may have enabled substantial expansion of NE as a major neurotransmitter.

To provide functional data to support these analyses, we directly measured DA, NE, and 5-HT levels in brain extracts of a diverse panel of chordate species around these gene duplication events (Supplementary Fig. 32). In amphioxus heads, only DA is observed (180 ng DA/g wet tissue) with no detectable NE. Further along in evolutionary development, DA is still the dominant monoamine neurotransmitter, at a 7:1 ratio over NE in lampreys (142 ng/g DA vs 20 ng/g NE). Interestingly, NE levels in lamprey muscle (107 ng/g) are approximately 5-fold higher than in brain. Sharks constitute a transition point, where one species, dogfish (Mustelus canis), has approximately 3-fold higher NE compared to DA, but two other species show much higher levels of DA over NE. Finally, all teleosts tested, including zebrafish, possess NE levels that far exceed DA levels in their brains. Taken together, the data indicate that NE, which is biosynthesized by the copper-dependent enzyme DBH, is the newest addition to the group of monoamine neurotransmitters found in the CNS, starting around the Gnathostome stage and emerging at the same time as the expansion of the ATP7 copper transporter family.

DISCUSSION

The LC is a unique brain structure, appearing only in vertebrates, which has evolved to be a hub for regulating a diverse array of behaviors spanning sleep, arousal, attention, learning, memory, and emotion. As such, a central question in neurobiology is the chemical origin of LC development. At the molecular level, the LC is distinguished as the principal source of NE synthesis in the CNS, mediated exclusively by the copper-dependent enzyme DBH. Recognizing that a central tenet of metals in biology is that they must be acquired because they can neither be created nor destroyed under physiological conditions, we hypothesized that copper itself might represent the most basic chemical origin of LC development.

Major changes of both catecholamine and copper transport systems occurred in parallel after the Cambrian explosion *ca.* 540 million years ago. During this period, NE overtook DA as the dominant catecholamine in the CNS, where a small number of LC cells are especially equipped to synthesize steady-state NE levels that far surpass the other monoamine neurotransmitters DA and 5-HT. Through phylogenetic analysis, we identified parallel evolution of genes in copper homeostasis and LC-NE pathways, specifically the duplication of *atp7* into *atp7a* and *atp7b* coinciding with the rise of the LC-NE system beginning in the Gnathostome stage. During early vertebrate evolution, it has been suggested that there were two rounds of whole genome duplications, and possibly a third before the split of agnathans from the rest of the vertebrates[46,47]. The gene encoding ATP7A, which metalates DBH, appeared in Agnatha, potentially resulting from one of these gene duplication events. This major change in copper homeostasis is accompanied by the appearance of the NE transport system for regulating synaptic NE levels through presynaptic re-uptake (NET/Slc6a2). Notably, NET has not been detected in any species before Gnathostomata. In Gnathostomata, only a partial NET sequence is predicted in the elephant shark (Callorhinchus milii) genome. These newly acquired genes in early vertebrates likely enabled the rise of NE as a major neurotransmitter in Gnathostomata. The functional differentiation between the two ATP7 paralogues[48] might have enabled tissue-specific copper homeostasis that would facilitate diversification of the function of NE, and possibly account for evolution of the specialized structure of the LC.

Our findings support the concept that distributions of copper in the CNS are highly spatially and temporally regulated. Indeed, direct metal imaging with LA-ICP-MS, accompanied by a unique pair of fluorescent chemical probes that enable labile copper imaging in the brain *in vivo*, reveals that copper distributions are developmentally regulated: brain copper levels steadily increase during development, with neuropils and fascicles showing the most dramatic changes. In contrast, another major transition metal, zinc, is enriched in cell body regions and barely detectable in neuropils. Notably, the spatial resolution afforded by imaging enables detection of specific deficiencies in neurite copper in the brains of a missense mutant of ATP7A, *Cal*^{gw71}, where bulk measurements of copper in the entire animal show negligible differences between mutants and wildtype siblings.

We further show that copper is required for normal rest–activity and arousal behaviors in fish. Indeed, LC-NE circuitry has been implicated in sleep and arousal in mammals[20,49] and related behaviors in fish[50], and our data reveal that the LC serves an important role in

stabilizing both rest and activity states. Since *dbh* gene transcription reaches peak levels just before dawn, production of the copper-dependent DBH protein prior to waking may be particularly affected by impaired copper homeostasis, leading to impaired NE synthesis. In line with this reasoning, we found that *Cal*^{gw71} ATP7A mutants exhibiting brain copper deficiency have pronounced and specific defects in the rest–activity transition, despite being indistinguishable from their wildtype siblings in gross morphology, growth, fertility. The copper-dependent rest–activity defect can be rescued pharmacologically using NET inhibitors that increase synaptic NE levels, linking the need for copper to DBH activity and NE production and supporting a model where copper homeostasis is indeed essential for LC function through a CTR1-ATP7A-DBH-NE molecular pathway.

This work establishing copper as an elemental chemical origin of the LC and regulator of LC-mediated sleep-related behavior has broader implications, as clinical copper dysregulation can cause a wide range of neurological symptoms beyond sleep disorders, including depression, mental retardation, and neurodegeneration[20]. For example, in the copper-dependent genetic disorder Wilson's disease, 50% of the patients are diagnosed with neurological symptoms with severity uncorrelated with the severity of the copper-dependent liver damage[39]. More complex neurodegenerative disorders, including Alzheimer's, Parkinson's, and Huntington's diseases along with ALS and autism, exhibit alterations in copper homeostasis and thus motivate further investigations of the metallophysiology/metallopathology interface for both fundamental research and new therapeutic intervention.

ONLINE METHODS

Synthesis of CF4 and Ctrl-CF4-S2

See Supplementary Note.

Zebrafish lines

Zebrafish of the AB and TL strains were raised and bred at 28.5°C on a 14 h light/10 h dark cycle. Embryos were produced by natural crosses and staged by hours, or days post fertilization (hpf, or dpf) following AUP in compliance with zebrafish ethical regulations and approved by the UC Berkeley ACUC. Embryos were raised in copper-free E3 or egg water (60μg/ml Instant Ocean Sea Salt in distilled water). Instant Ocean Sea Salt contains approximately 1.8 μmol/kg of copper[51]. Designations of mutant and transgenic lines adhered to nomenclature rules set according to http://zfin.org. The following mutants or transgenic lines were used: *Calamity*^{gw71} mutants (*Cal*^{gw71})[38], nacre/*mitfa*(−/−) mutants[52], *Tg(elavl3:GCaMP5)*[53], *Tg(dbh:mCherry),* and *Tg(dbh:eGFP)*[43]. Genotyping of *Calamity*^{gw71} mutants was carried out as described previously[38].

In vivo labeling

Zebrafish embryos in nacre background were incubated in 10 μM CF4 or Ctrl-CF4-S2 with 1% DMSO in E3 solution overnight. Embryos were washed, embedded in 2% low-melting agarose, and imaged at 3 dpf.

Fluorescence microscopy imaging

Larvae were embedding in 2% agarose and imaged by laser scanning confocal microscopy (Zeiss, using a 20x/NA1.0 water-dipping objective) at 0.5μm per step. Z-stacks were obtained at 1024p with a pinhole of 1 Airy unit at 488 nm excitation. Channels for 488 nm, 561 nm, and transmitted light images were acquired simultaneously.

2-Photon laser ablation assays

For behavioral studies in LC-ablated animals, *Tg(dbh-mCherry; elavl3:GCaMP5)* larvae were mounted in agarose at 3 dpf, and LC cells were bilaterally removed by 2-photon ablation on a Zeiss LSM 880 confocal microscope. The 800-nm ablation laser (Coherent Chameleon Vision) was rastered over LC somata guided by mCherry fluorescence, and the progress of the ablation was monitored by simultaneously imaging Ca^{2+} responses from GCaMP5 and microcavitation with transmitted light. In this way, LC cells were selectively destroyed with very little collateral damage. Larvae were unmounted and allowed to recover for at least 24 hr prior to behavior experiments. LC-intact siblings were subjected to the same rearing conditions to control for rate of development. Following behavior experiments, ablated animals were re-imaged to confirm complete loss of LC.

Liquid sample ICP-MS

Fish was euthanized in tricaine or ice following standard protocol. Tissues were quickly harvested and weighed, then digested 1 mL trace-metals grade concentrated nitric acid per 100 mg of tissue, at room temperature on a rotator in 1.5 mL tubes (Sarstedt). Digested samples were diluted in 2% nitric acid with 1 ppm Ga solution as internal and analyzed with iCAP-Qc ICP-MS (Thermal Fischer).

Laser Ablation Inductively Coupled Plasma Mass Spectrometry (LA-ICP-MS)

Zebrafish embryos were raised in Instant Ocean to 2, 4, or 6 days post fertilization (dpf). Embryos were euthanized and immediately embedded in Optimal Cutting Temperature (OCT) mounting media (Tissue Tek) in cryomolds (Tissue Tek). The embedded embryos were immediately frozen in a dry ice/isopentane bath and stored at −80° C until sectioning. For 4–18 hours before sectioning, the embedded embryos were equilibrated to −20° C. The embryos were sectioned into 20 μm slices using Leica CM1950 and adhered to Superfrost slides (Thermo Fisher). The slices were air-dried and stored at room temperature until analysis. Laser ablation was performed on an NWR213 laser with a TV2 sample chamber (ESI, Bozeman, MT) using the following parameters: Spot size: 6 μm; Fluence: 2.3 J cm^{-2}; Stage speed: 15 μm s^{-1}; Firing rate: 20 Hz; He flow: 800 mL min^{-1}; Pattern spacing: 6 μm. Using these parameters, the tissue was fully ablated but the glass slide remained undamaged. The ablated material was introduced by gas flow into an iCAP-Qc ICP-MS (Thermo Fisher) and analyzed for ^{63}Cu or ^{66}Zn content using a 0.4 sec dwell time in standard acquisition mode. The resulting mass spectrometry traces and laser log files were processed in Igor Pro using the Iolite application. The Trace Elements data reduction scheme was used in Semi-quantitative mode using ^{63}Cu or ^{66}Zn as the reference trace and a custom matrix-matched standard to convert mass spectrometer counts to metal concentration.

Preparation of matrix-matched LA-ICP-MS standards

Salmon muscle (30 mL of packed tissue) was digested by adding 10 mL of protease solution (0.25% trypsin, 10 mM EDTA, 0.1X PBS) and 48 μL of Collagenase P (100 mg mL-1 in HBSS) in a 50 mL plastic conical tube. The solution was mixed with a plastic spatula (to minimize metal contamination) and incubated at 28° C for 4 hours with periodic mixing. The tissue was stored at 4°C overnight. The next day, the tissue was warmed to 28° C for an additional 6 hours of digestion and homogenized in a Dounce homogenizer using 10 passes until the tissue was gooey and smooth. The tissue was separated into 500 μL aliquots in 1.5 mL Sarstedt tubes and frozen at −20° C until metal addition. A solution of $CuCl_2$, $ZnCl_2$, Fe(citrate), $CaCl_2$, $MgCl_2$, and KCl (10,000 ppm each) was prepared in water. Dilutions of 5000, 1000, 500, 100, 50, and 10 ppm were made in water. Each dilution was mixed 1:10 with an aliquot of tissue (50 μL metal mixture per 500 μL tissue) and mixed with a hand-held mechanical homogenizer. To remove bubbles, the standards were centrifuged at 16,000 x g at room temperature for 2 hours. Any resulting supernatant was removed, and the vials were frozen in a dry ice/isopentane bath and stored at −80° C until sectioning. Before sectioning, the standards were cut in half vertically. One half was sectioned into 20 μm slices using a CRYOSTAT (Leica CM1950) and adhered to Superfrost slides (Thermo Fisher), air-dried, and stored at room temperature until analysis. The other half was divided into three parts for liquid ICP-MS analysis. The samples for liquid analysis were weighed in 1.5 mL tubes (Sarstedt) and combined 1:1 (w/v) with concentrated nitric acid (BDH Aristar Ultra). After overnight incubation at room temperature, samples were diluted into 2% HNO_3 (prepared from concentrated acid in milliQ water) and doped with a gallium internal standard (Inorganic Ventures, 20 ppb final concentration). The metal content was determined by measuring ^{63}Cu and ^{66}Zn using a Thermo Fisher iCAP-Qc ICP-MS in Kinetic Energy Discrimination (KED) mode with the He flow set to 4.426 mL min^{-1}. Measurements were normalized to a standard curve of known metal concentrations doped with 20 ppb Ga. The standard curve was diluted from CMS-5 (Inorganic Ventures).

Rest-activity and acoustic startle response assays

Embryos in AB strain background were raised in E3 under a 14 hr light / 10 hr dark light cycle at 28.6° C until 4 dpf. Larvae with fully inflated swim bladders were then transferred individually into 48-well plates in 900 μL volume of E3 with or without drug treatment, and placed in a light controlled imaging arena maintained under the same 14 hr light / 10 hr dark with ambient light on between 9:00 am and 11:00 pm. Recording was conducted using a custom-built apparatus. Film resolution of 1388x1240p corresponded to 140x140p per well. Larvae were filmed between 4.5 and 6.5 dpf for 1 min (1 fps) at intervals of 4.5 minutes for rest-activity assays.

For acoustic startle response assay, sound was delivered by two speakers (Visaton SC5.9) coupled to the multi-well plate via the plate-holder platform were driven by a 15W amplifier. The acoustic stimuli were 900Hz square waves of ~3ms duration, ranging across six different volume levels of approximately 68dB, 73.5dB, 79dB, 84.5dB, 90dB, and 95.5dB. Each of the six volumes were randomly delivered three-times per level in the morning (~10am) and night (~2am). Larvae were filmed at 30fps.

Behavioral analysis

Activity was quantified by summing pixel changes between frames using custom scripts in Fiji/ImageJ and Matlab (MathWorks). Cohort mean activity traces were obtained from mean of normalized individual activity. Animals with no inflated swim bladder or no activity (<10% population) were excluded from analysis. An escape event was calculated using the difference in pixel values between frames. An acoustic startle response was counted if the difference of the summated pixel values from the two frames immediately following the stimulus was statistically higher ($P < 0.01$, 2-sample t-test) than the distribution of pixel-change values taken from the non-escape portion of spontaneous activity in the movies. This analysis method was confirmed by visual inspection of the behavioral movies. Data used are pooled from fish bred crosses over three generations. Wildtype controls are either genotyped siblings or cousins of the *Cal*$^{gw71-/-}$ mutants.

In situ hybridization assays

A fragment of DBH were amplified from cDNA by PCR and cloned into pCR2.1 vector. The following primers were used: 5′-CTCCTCGGGCATTCGTTTAT-3′; and 5′-CCTCTGTAGGGCTGTCATTATTAG-3′. Plasmids containing ctr1 and atp7a cDNA fragments were provided kindly by Dr Jonathan Gitlin. *In situ* hybridization was performed as described previously[54]. A fragment of ctr1, atp7a and dbh was used to generate sense and antisense riboprobes with digoxigenin-labeled UTP. Probes were hydrolyzed to yield 200-base fragments. Embryos/larvae were sectioned in gelatin/albumin at 20 μm coronally on a vibratome (Leica). For fluorescent *in situ* hybridyzation, anti-DIG POD (Roche) was used at 1:400 dilution followed by tyramid amplification.

Immunohistochemistry

Immunohistochemistry stainings were performed as described previously[54]. Anti-GFP (Invitogen, A-6455) was used at 1:4000 for wholemount immunohistochemistry: anti-mCherry (Chemicon, AB356482) was used at 1: 1200 for frozen-section immunohistochemistry

Real time PCR analysis

Triplicates of 30 Larvae from 5 dpf to 6 dpf were collected every 4 hours and frozen in RNAlater (ThermoFisher). RNA was extract with RNAasy Plus (Qiagen), quantified and then reverse-transcribed with iScript (BioRad). Real-time PCR was performed using iQ SYBRGreen following standard protocol on CFX^{TM} Real-Time system (BioRad). The following primers were used:

dbh: 5′-CTTGGGCTGGTCTACACTC-3′; 5′-TGGGAGGCAAAGATGTGTATG-3′

atp7a: 5′-TGACCTGTGGCTCCTGTGTA-3′; 5′-CTGGTGTTGATGTAGCGTTTG-3′

ctr1: 5′-GTGAACGTGCGCTACAACTC-3′; 5′-CCACCACTTGGATGATGTGA-3′

EF1a: 5′-CTGGAGGCCAGCTCAAACAT-3′; 5′-ATCAAGAAGAGTAGTACCGCTAGCATTAC-3′

b-actin: 5′-CGAGCTGTCTTCCCATCC A-3′; 5′-TCACCAACGTAGCTGTCTTTCTG-3′

Phylogenetic analysis

The trees were built based on ensemble methods[55]. Data were exported and plotted with Matlab.

Catecholamine analysis

Amphioxus, shark and ray brain samples were purchased from Marine Biological laboratory and Gulf Specimen. Sticklebacks were kindly provided by Dr. Craig Miller. Archer fish were kindly provided by Dr. Ronen Segev. Brains were quickly dissected, weighted, and homogenized in 0.1 M PCA solution. After centrifuging, supernatants were analyzed by HPLC-ECD for norepinephrine (NE) and dopamine (DA) or LC/MS/MS for serotonin (5-HT) by BASi.

Briefly, serotonin is detected from fish tissue extract by LC/MS/MS. Glycinexylidide was added to the clear fish tissue extract as internal standard before the injection. After vortex-mixing and centrifugation, the sample was injected into an LC-MS/MS system using a PFP column with a gradient water/acetonitrile/formic acid mobile phase. NE and DA were detected from fish tissue extract by LC/EC. 3,4-Dihydroxybenzylamine was added to the clear fish tissue extract as internal standard before the injection. After vortex-mixing and centrifugation, the sample was injected into an LC/EC system using a Gemini C18 column with a EDTA/SDS/phosphate buffer mobile phase.

Statistics and reproducibility

Statistical tests were conducted using GraphPad Prism7 and Matlab (2016a). In Figure 6 Bars represent mean ± s.e.m. Figure 6g, shaded region is s.e.m. of population.

Code availability

Codes supporting this study are available upon request.

Data availability

The data that support the findings of this study are available from the corresponding authors upon request.

Life sciences reporting summary

Further information on experimental design and reagents is available in the Life sciences reporting summary.

Supplementary Material

Refer to Web version on PubMed Central for supplementary material.

Acknowledgments

We thank the NIH (GM79465 to C.J.C. and PN2EY018241 to E.Y.I.) for providing funding for this work. C.J.C. is an Investigator of the Howard Hughes Medical Institute and a CIFAR Senior Fellow. C.M.A. was partially supported by a Hertz Foundation Graduate Fellowship and a Chemical Biology Training Grant from the NIH (T32 GM066698). We thank Prof. A. Thomas Look and Prof. Jonathan Gitlin for providing plasmids and transgenic fish lines, Prof. Craig Miller and Prof. Ronen Segev for providing fish samples, and Rock Feng and Raphael Fish for assistance with pilot experiments. Experiments at the CRL Molecular Imaging Center were supported by the Helen Wills Neuroscience Institute.

References

1. Bush AI. Metals and neuroscience. Curr Opin Chem Biol. 2000; 4:184–191. [PubMed: 10742195]
2. Que EL, Domaille DW, Chang CJ. Metals in neurobiology: probing their chemistry and biology with molecular imaging. Chem Rev. 2008; 108:1517–1549. DOI: 10.1021/cr078203u [PubMed: 18426241]
3. Barnham KJ, Masters CL, Bush AI. Neurodegenerative diseases and oxidative stress. Nat Rev Drug Discov. 2004; 3:205–214. DOI: 10.1038/nrd1330 [PubMed: 15031734]
4. Kaler SG. ATP7A-related copper transport diseases-emerging concepts and future trends. Nat Rev Neurol. 2011; 7:15–29. DOI: 10.1038/nrneurol.2010.180 [PubMed: 21221114]
5. Madsen E, Gitlin JD. Copper and iron disorders of the brain. Annu Rev Neurosci. 2007; 30:317–337. DOI: 10.1146/annurev.neuro.30.051606.094232 [PubMed: 17367269]
6. Zlatic S, Comstra HS, Gokhale A, Petris MJ, Faundez V. Molecular basis of neurodegeneration and neurodevelopmental defects in Menkes disease. Neurobiol Dis. 2015; 81:154–161. DOI: 10.1016/j.nbd.2014.12.024 [PubMed: 25583185]
7. Duncan C, White AR. Copper complexes as therapeutic agents. Metallomics. 2012; 4:127–138. DOI: 10.1039/c2mt00174h [PubMed: 22187112]
8. Lutsenko S, Bhattacharjee A, Hubbard AL. Copper handling machinery of the brain. Metallomics. 2010; 2:596–608. DOI: 10.1039/c0mt00006j [PubMed: 21072351]
9. Prohaska JR. Functions of trace elements in brain metabolism. Physiol Rev. 1987; 67:858–901. [PubMed: 3299411]
10. Warren PJ, Earl CJ, Thompson RH. The distribution of copper in human brain. Brain. 1960; 83:709–717. [PubMed: 13783233]
11. Zecca L, et al. The role of iron and copper molecules in the neuronal vulnerability of locus coeruleus and substantia nigra during aging. Proc Natl Acad Sci U S A. 2004; 101:9843–9848. DOI: 10.1073/pnas.0403495101 [PubMed: 15210960]
12. German DC, et al. Disease-specific patterns of locus coeruleus cell loss. Ann Neurol. 1992; 32:667–676. DOI: 10.1002/ana.410320510 [PubMed: 1449247]
13. Braak H, Del Tredici K. Where, when, and in what form does sporadic Alzheimer's disease begin? Curr Opin Neurol. 2012; 25:708–714. DOI: 10.1097/WCO.0b013e32835a3432 [PubMed: 23160422]
14. Cotruvo JA Jr, Aron AT, Ramos-Torres KM, Chang CJ. Synthetic fluorescent probes for studying copper in biological systems. Chem Soc Rev. 2015; 44:4400–4414. DOI: 10.1039/c4cs00346b [PubMed: 25692243]
15. Nevitt T, Ohrvik H, Thiele DJ. Charting the travels of copper in eukaryotes from yeast to mammals. Biochim Biophys Acta. 2012; 1823:1580–1593. DOI: 10.1016/j.bbamcr.2012.02.011 [PubMed: 22387373]
16. Robinson NJ, Winge DR. Copper metallochaperones. Annu Rev Biochem. 2010; 79:537–562. DOI: 10.1146/annurev-biochem-030409-143539 [PubMed: 20205585]
17. O'Halloran TV, Culotta VC. Metallochaperones, an intracellular shuttle service for metal ions. J Biol Chem. 2000; 275:25057–25060. DOI: 10.1074/jbc.R000006200 [PubMed: 10816601]
18. Banci L, et al. Affinity gradients drive copper to cellular destinations. Nature. 2010; 465:645–648. DOI: 10.1038/nature09018 [PubMed: 20463663]

19. Lutsenko S, Barnes NL, Bartee MY, Dmitriev OY. Function and regulation of human copper-transporting ATPases. Physiol Rev. 2007; 87:1011–1046. DOI: 10.1152/physrev.00004.2006 [PubMed: 17615395]
20. Aston-Jones G, Waterhouse B. Locus coeruleus: From global projection system to adaptive regulation of behavior. Brain Res. 2016; 1645:75–78. DOI: 10.1016/j.brainres.2016.03.001 [PubMed: 26969408]
21. Sara SJ. The locus coeruleus and noradrenergic modulation of cognition. Nat Rev Neurosci. 2009; 10:211–223. DOI: 10.1038/nrn2573 [PubMed: 19190638]
22. Moret C, Briley M. The importance of norepinephrine in depression. Neuropsychiatr Dis Treat. 2011; 7:9–13. DOI: 10.2147/NDT.S19619 [PubMed: 21750623]
23. Kaufman S, Friedman S. Dopamine-Beta-Hydroxylase. Pharmacol Rev. 1965; 17:71–100. [PubMed: 14294032]
24. Mangold JB, Klinman JP. Mechanism-based inactivation of dopamine beta-monooxygenase by beta-chlorophenethylamine. J Biol Chem. 1984; 259:7772–7779. [PubMed: 6547439]
25. Ash DE, Papadopoulos NJ, Colombo G, Villafranca JJ. Kinetic and spectroscopic studies of the interaction of copper with dopamine beta-hydroxylase. J Biol Chem. 1984; 259:3395–3398. [PubMed: 6323422]
26. Kim BE, Nevitt T, Thiele DJ. Mechanisms for copper acquisition, distribution and regulation. Nat Chem Biol. 2008; 4:176–185. DOI: 10.1038/nchembio.72 [PubMed: 18277979]
27. Scatton B, Javoy-Agid F, Rouquier L, Dubois B, Agid Y. Reduction of cortical dopamine, noradrenaline, serotonin and their metabolites in Parkinson's disease. Brain Res. 1983; 275:321–328. [PubMed: 6626985]
28. Hornby PJ, Piekut DT. Immunoreactive dopamine beta-hydroxylase in neuronal groups in the goldfish brain. Brain Behav Evol. 1988; 32:252–256. [PubMed: 3069181]
29. Ekstrom P, Reschke M, Steinbusch H, van Veen T. Distribution of noradrenaline in the brain of the teleost Gasterosteus aculeatus L.: an immunohistochemical analysis. J Comp Neurol. 1986; 254:297–313. DOI: 10.1002/cne.902540304 [PubMed: 3540043]
30. Parent A. Functional Anatomy and Evolution of Monoaminergic Systems. American Zoologist. 1984; 24:783–790.
31. Hirayama T, Van de Bittner GC, Gray LW, Lutsenko S, Chang CJ. Near-infrared fluorescent sensor for in vivo copper imaging in a murine Wilson disease model. Proc Natl Acad Sci U S A. 2012; 109:2228–2233. DOI: 10.1073/pnas.1113729109 [PubMed: 22308360]
32. Heffern MC, et al. In vivo bioluminescence imaging reveals copper deficiency in a murine model of nonalcoholic fatty liver disease. Proc Natl Acad Sci U S A. 2016; 113:14219–14224. DOI: 10.1073/pnas.1613628113 [PubMed: 27911810]
33. Hare DJ, New EJ, de Jonge MD, McColl G. Imaging metals in biology: balancing sensitivity, selectivity and spatial resolution. Chem Soc Rev. 2015; 44:5941–5958. [PubMed: 26505053]
34. Ackerman CM, Lee S, Chang CJ. Analytical Methods for Imaging Metals in Biology: From Transition Metal Metabolism to Transition Metal Signaling. Anal Chem. 2017; 89:22–41. DOI: 10.1021/acs.analchem.6b04631 [PubMed: 27976855]
35. Colburn RW, Maas JW. Adenosine triphosphate--metal--norepinephrine ternary complexes and catecholamine binding. Nature. 1965; 208:37–41. [PubMed: 5886682]
36. Sato M, Ohtomo K, Daimon T, Sugiyama T, Iijima K. Localization of copper to afferent terminals in rat locus ceruleus, in contrast to mitochondrial copper in cerebellum. J Histochem Cytochem. 1994; 42:1585–1591. [PubMed: 7983358]
37. Gaier ED, Eipper BA, Mains RE. Copper signaling in the mammalian nervous system: synaptic effects. J Neurosci Res. 2013; 91:2–19. DOI: 10.1002/jnr.23143 [PubMed: 23115049]
38. Madsen EC, Gitlin JD. Zebrafish mutants calamity and catastrophe define critical pathways of gene-nutrient interactions in developmental copper metabolism. PLoS Genet. 2008; 4:e1000261. [PubMed: 19008952]
39. Zimbrean PC, Schilsky ML. Psychiatric aspects of Wilson disease: a review. Gen Hosp Psychiatry. 2014; 36:53–62. DOI: 10.1016/j.genhosppsych.2013.08.007 [PubMed: 24120023]
40. Pantoja C, et al. Neuromodulatory Regulation of Behavioral Individuality in Zebrafish. Neuron. 2016; 91:587–601. DOI: 10.1016/j.neuron.2016.06.016 [PubMed: 27397519]

41. Chen S, et al. Light-Dependent Regulation of Sleep and Wake States by Prokineticin 2 in Zebrafish. Neuron. 2017; 95:153–168e156. DOI: 10.1016/j.neuron.2017.06.001 [PubMed: 28648499]
42. Lein ES, et al. Genome-wide atlas of gene expression in the adult mouse brain. Nature. 2007; 445:168–176. DOI: 10.1038/nature05453 [PubMed: 17151600]
43. Zhu S, et al. Activated ALK collaborates with MYCN in neuroblastoma pathogenesis. Cancer Cell. 2012; 21:362–373. DOI: 10.1016/j.ccr.2012.02.010 [PubMed: 22439933]
44. Deisseroth K. Circuit dynamics of adaptive and maladaptive behaviour. Nature. 2014; 505:309–317. DOI: 10.1038/nature12982 [PubMed: 24429629]
45. Caballero J, Nahata MC. Atomoxetine hydrochloride for the treatment of attention-deficit/hyperactivity disorder. Clin Ther. 2003; 25:3065–3083. [PubMed: 14749146]
46. Dehal P, Boore JL. Two rounds of whole genome duplication in the ancestral vertebrate. PLoS Biol. 2005; 3:e314. [PubMed: 16128622]
47. Panopoulou G, Poustka AJ. Timing and mechanism of ancient vertebrate genome duplications -- the adventure of a hypothesis. Trends Genet. 2005; 21:559–567. DOI: 10.1016/j.tig.2005.08.004 [PubMed: 16099069]
48. Dmitriev O, et al. Solution structure of the N-domain of Wilson disease protein: distinct nucleotide-binding environment and effects of disease mutations. Proc Natl Acad Sci U S A. 2006; 103:5302–5307. DOI: 10.1073/pnas.0507416103 [PubMed: 16567646]
49. Li SB, Jones JR, de Lecea L. Hypocretins, Neural Systems, Physiology, and Psychiatric Disorders. Curr Psychiatry Rep. 2016; 18:7. [PubMed: 26733323]
50. Singh C, Oikonomou G, Prober DA. Norepinephrine is required to promote wakefulness and for hypocretin-induced arousal in zebrafish. Elife. 2015; 4:e07000. [PubMed: 26374985]
51. Atkinson MJ, Bingman C. Elemental composition of commercial seasalts. Journal of Aquariculture and Aquatic Sciences. 1998; VIII:39–43.
52. Lister JA, Robertson CP, Lepage T, Johnson SL, Raible DW. nacre encodes a zebrafish microphthalmia-related protein that regulates neural-crest-derived pigment cell fate. Development. 1999; 126:3757–3767. [PubMed: 10433906]
53. Ahrens MB, Orger MB, Robson DN, Li JM, Keller PJ. Whole-brain functional imaging at cellular resolution using light-sheet microscopy. Nat Methods. 2013; 10:413–420. DOI: 10.1038/nmeth.2434 [PubMed: 23524393]
54. Xiao T, Baier H. Lamina-specific axonal projections in the zebrafish tectum require the type IV collagen Dragnet. Nat Neurosci. 2007; 10:1529–1537. DOI: 10.1038/nn2002 [PubMed: 17982451]
55. Vilella AJ, et al. EnsemblCompara GeneTrees: Complete, duplication-aware phylogenetic trees in vertebrates. Genome Res. 2009; 19:327–335. DOI: 10.1101/gr.073585.107 [PubMed: 19029536]

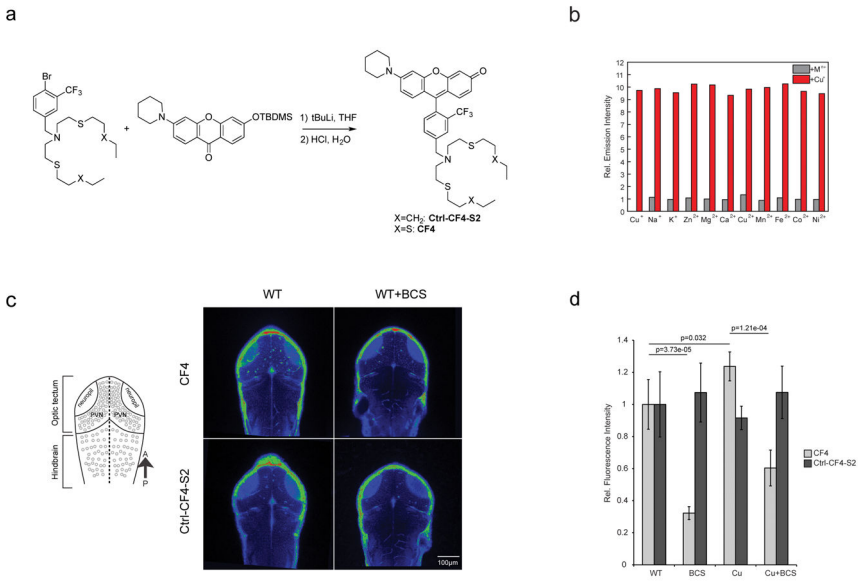

Figure 1. Molecular imaging reveals distributions of labile copper in the living brain

a, The synthesis of CF4 (**1**) and control probe Ctrl-CF4-S2 (**2**). **b**, Fluorescence responses of CF4 to various metal ions. Bars represent the final integrated fluorescence response (F_f) over the initial integrated emission (F_i). Grey bars represent the addition of an excess of the appropriate metal ion (2 mM for Na^+, Mg^{2+}, K^+, Ca^{2+}, and Zn^{2+}, 50 μM for all other cations) to a 2 μM solution of CF4. Red bars represent the subsequent addition of 2.5 μM Cu^+ to the solution. **c**, CF4 and Ctrl-CF4-S2 signals in 3 dpf zebrafish brain. dpf, days post fertilization; PVN, periventricular neurons. In the optic tectum, the PVN zone consists mostly of tectal neurons' cell bodies, while the neuropil consists mostly of neurites from retinal ganglion cells, tectal neurons, as well as other neurons with input to visual signal processing. These experiments have been repeated independently 3 times with similar results. **d**, Quantification of CF4 and Ctrl-CF4-S2 signals in the tectum region. N=12 for each group. Bars represent mean ± s.e.m. p values are two-sided t-tests.

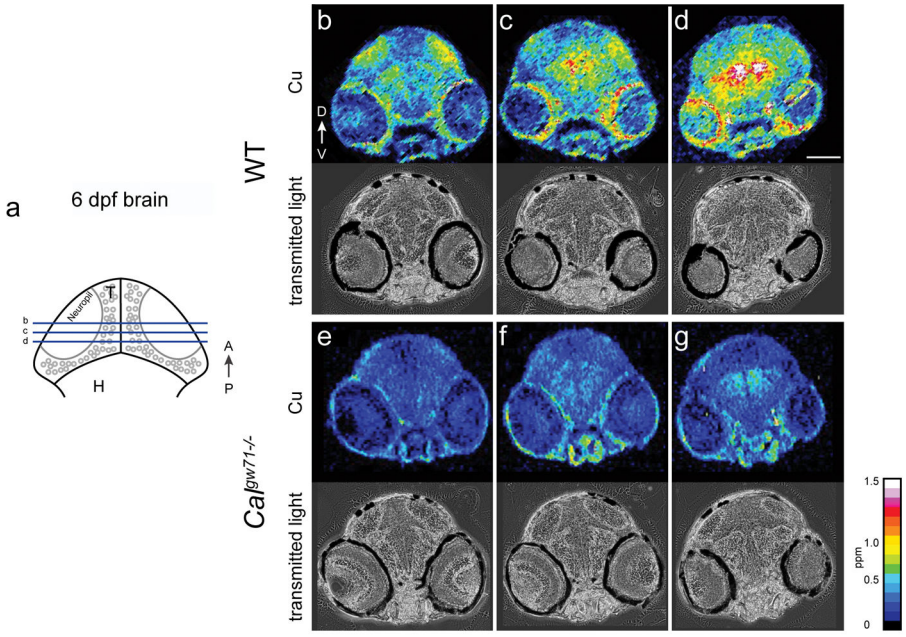

Figure 2. LA-ICP-MS imaging reveals heterogeneous copper distribution patterns in the brain during development

a, At 6 dpf, neurites innervate most brain regions. The lines indicate the three consecutive sections shown in **b**–**d. b**–**d**, Copper distributions measured by LA-LCP-MS of 6 dpf wildtype controls, in the sections indicated by the lines in **a. e**–**g**, Consecutive sections (analogous to **b**–**d**) of LA-ICP-MS images of 6 dpf *Calamity*^{gw71} mutants. Scale bar is 100 μm. T, tectum; H, hindbrain; P → A, posterior to anterior; V → D, ventral to dorsal. The colormetric scale bar represents copper concentrations ranging from 0–1.5 ppm. N=6 independent animals imaged for each genotype with similar results.

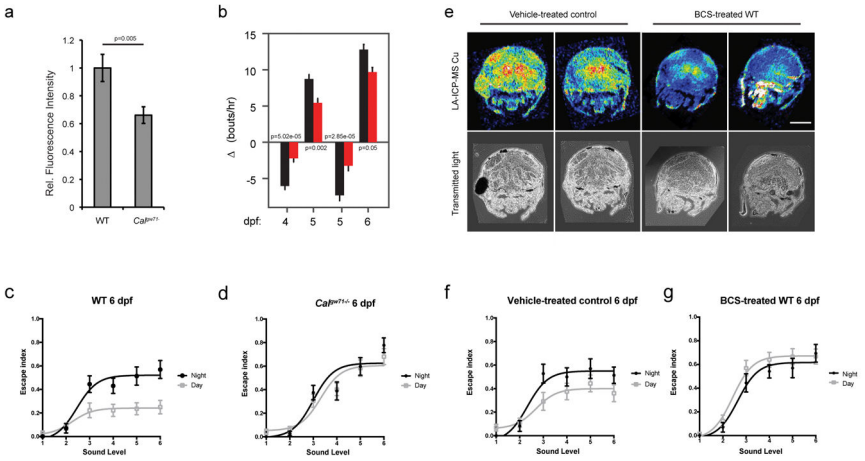

Figure 3. Dysregulation of brain copper homeostasis alters arousal and rest-activity behavior

a, Quantification of CF4 fluorescence signal intensity in brain of wildtype larvae and *Cal*^{gw71} mutant. N=12 brains for each group. Bars represent mean ± s.e.m. p value is two-sided Student's t-test. **b**, Change in frequency of swim bouts in WT (black, n=98) and *Cal*^{gw71} mutants (red, n=99) from 5 dpf to 6 dpf. Change in frequency of swim bouts recorded in 3 hr period preceding and following light transitions at dusk and dawn. Bars represent mean ± s.e.m. p values are two-sided Student's t-test. **c**, Comparison of stimulus response curves to sound using acoustic startle response (ASR) assay at night (black line) and day (grey line) of WT (n=24). P<0.0001 by extra sum-of-squares F test. **d**, Comparison of stimulus response curves to sound at night (black line) and day (grey line) of *Cal*^{gw71} mutants (n=24). P=0.1 by extra sum-of-squares F test. Bars represent mean ± s.e.m. **c** and **d** are tested with 6 dpf larvae. **e**, LA-ICP-MS images of copper distribution of 6 dpf larval brain sections showing BCS-treated larvae have decreased brain copper compared to their control group. N=6 for each group. **f**, Comparison of stimulus response curves to sound at night (black line) and day (grey line) of vehicle-treated controls (n=24). P<0.0001 by extra sum-of-squares F test. **g**, Comparison of stimulus response curves to sound at night (black line) and day (grey line) of BCS-treated larvae (n=24). P=0.32 by extra sum-of-squares F test. **f** and **g** are tested with 6 dpf larvae.

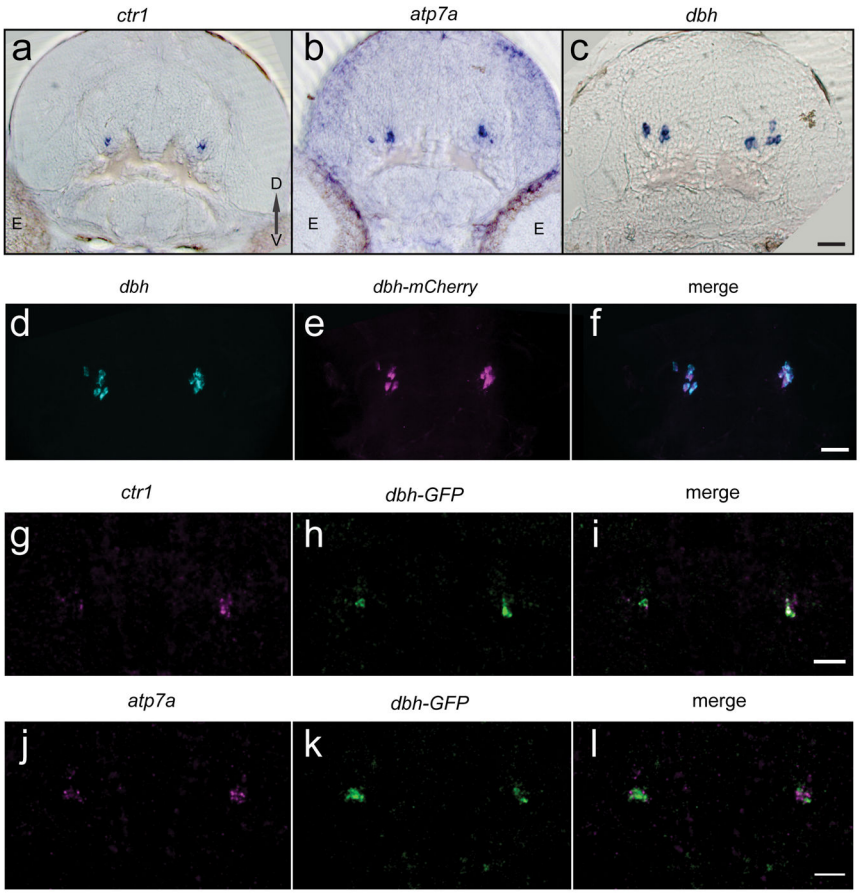

Figure 4. Copper transporter gene expression is highly and specifically enriched in LC

a–**c**, Coronal sections of 3 dpf brains using *in situ* hybridization to label *ctr1* (**a**), *atp7a* (**b**), and *dbh* (**c**). **d**–**f**, Dorsal views of a 5 dpf *Tg(dbh:mCherry)* larval brain. **d**, *dbh* mRNA expression was detected by fluorescent *in situ* hybridization. **e**, Anti-mCherry immunostaining. **f**, Merged image from **d** and **e** showing mCherry is expressed by all *dbh*-positive cells in LC. **g**–**i**, Horizontal optical sections of a 3 dpf *Tg(dbh:eGFP)* fish labeled with fluorescent *in situ* hybridization for *ctr1*. **g**, *ctr1* mRNA in magenta. **h**, Anti-GFP labeling showing LC neurons. **i**, Merged image of **g** and **h. j**–**l**, Horizontal optical sections of a 3 dpf *Tg(dbh:eGFP)* fish labeled with fluorescent *in situ* hybridization for *atp7a*. **j**, *atp7a* mRNA in magenta. **k**, anti-GFP labeling showing LC neurons. **l**, Merged image of **j** and **k**. Scale bars are 20 μm. Each experiment was independently replicated three times.

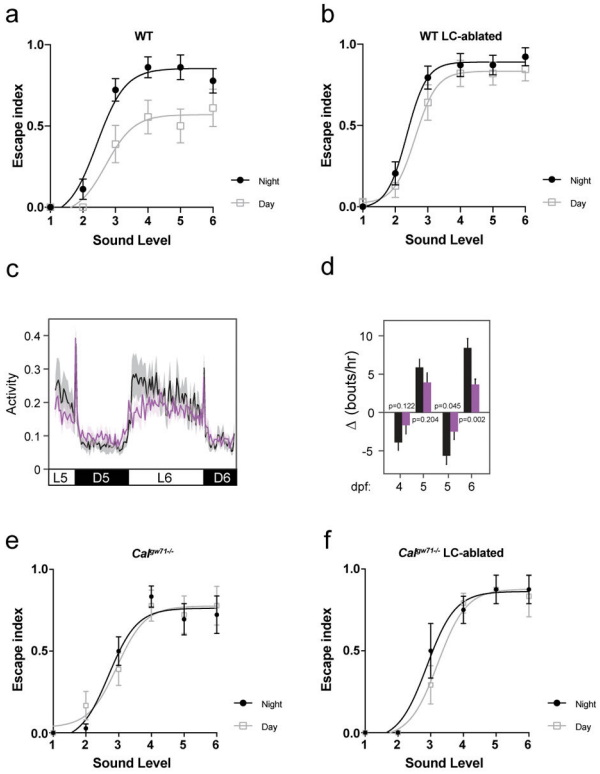

Figure 5. LC-NE circuitry mediates copper-regulated behaviors

a, Comparison of stimulus response curves to sound at night (black line) and daytime (grey line) of WT sham controls (n=12). P<0.0001 by extra sum-of-squares F test. **b**, Comparison of stimulus response curves to sound at night (black line) and daytime (grey line) of LC-ablated WT (n=13). P=0.35 by extra sum-of-squares F test. **c**, Average activity for wildtype (black, n=38) and LC-ablated siblings (purple, n=34) from 5.2 dpf to 6.7 dpf. Light/dark cycle is indicated at bottom. For all traces, shaded region is s.e.m. of the population. **d**, Change in frequency of swim bouts recorded in a 3 hr period preceding and following light transitions at dusk and dawn. Bars represent mean ± s.e.m. p values are two-sided Student's t-test. **e**, Comparison of stimulus response curves to sound at night (black line) and day (grey line) of *Cal*^{gw71} mutant sham controls (n=12). P=0.84 by extra sum-of-squares F test. **f**, Comparison of stimulus response curves to sound at night (black line) and day (grey line) of LC-ablated *Cal*^{gw71} mutants (n=8). P=0.56 by extra sum-of-squares F test. Bars represent mean ± s.e.m.

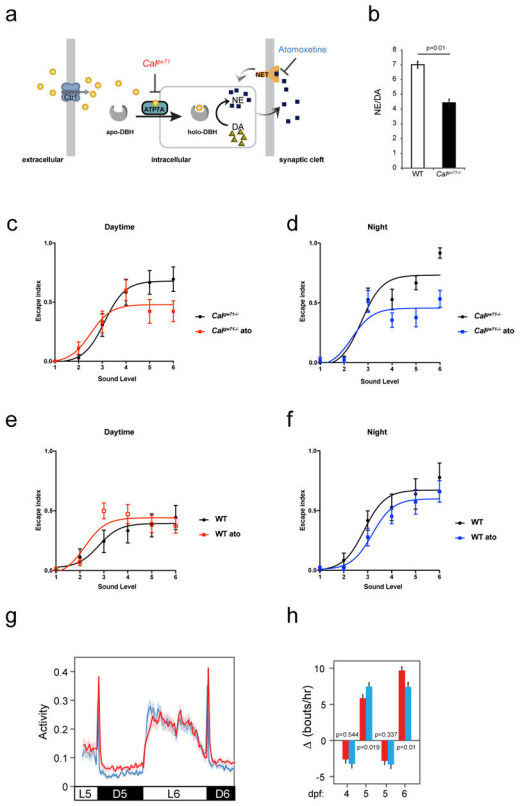

Figure 6. Copper transporter gene duplication coincides with the rise of brain NE levels and NE transport in Gnathostomata

a, Schematic drawing of the norepinephrine (NE) synapse, in which ATP7A metalates DBH with copper. Copper-loaded DBH converts dopamine (DA) to NE inside synaptic vesicles. After NE is released into the synaptic cleft, SCL6A2/NET selectively uptakes NE back into presynaptic terminals to ensure rapid turnover of NE. **b**, *Cal*^{gw71} mutants exhibit a lower NE to DA ratio for 6 dpf larvae. Triplicates of 40 larvae were measured by HPLC-ECD for each group. Bars represent mean ± s.e.m. p value is two-sided Student's t-test. **c**, Comparison of stimulus response curves to sound during daytime of *Cal*^{gw71} mutants (black line) and *Cal*^{gw71} mutants treated with 300 nM NET inhibitor atomoxetine (red line) (n=15 for each group). P < 0.0001. **d**, Comparison of stimulus response curves to sound during night of *Cal*^{gw71} mutants (black line) and *Cal*^{gw71} mutants treated with 300 nM NET inhibitor atomoxetine (blue line) (n=15 for each group). P < 0.0001. **e**, Comparison of stimulus response curves to sound during daytime of WT control (black line) and WT treated with 300 nM NET inhibitor atomoxetine (red line) (n=15 for each group). P =0.11. **f**, Comparison of stimulus response curves to sound during night of WT controls (black line) and WT treated with 300 nM NET inhibitor atomoxetine (blue line) (n=15 for each group). P=0.97. In **c**–**f**, p-values are extra sum-of-squares F test. **g**, Average activity of *Cal*^{gw71} larvae between 5.2 dpf and 6.7 dpf for untreated (red, n=146) and treated with 100 nM NET inhibitor atomoxetine (blue, n=108). **h**, Change in swim bout frequency for data in **g**. p-values are two-sided Student's t-test.